SLAC–PUB–4497
May 1988
T/E/AS

BOLOMETRIC DETECTION OF COLD DARK MATTER CANDIDATES: Some Material Considerations*

A. K. DRUKIER

Applied Research Corporation
8201 Corporate Drive, Suite 920
Landover, MD 20785

and

Physics Department
University of Maryland
College Park, MD 20742

and

KATHERINE FREESE†

Department of Astronomy
University of California
Berkeley, CA 94720

and

JOSHUA FRIEMAN

Stanford Linear Accelerator Center
Stanford University, Stanford, California 94309

Submitted to *Journal of Applied Physics*

---

* Work supported by the Department of Energy, contract DE–AC03–76SF00515.

† Present address: Dept. of Physics, Massachussetts Institute of Technology, Cambridge, MA 02139

ABSTRACT

We discuss the use of crystal bolometers to search for weakly interacting cold dark matter particles in the galactic halo. For particles with spin dependent nuclear interactions, such as photinos, Majorana neutrinos and higgsinos, we show that compounds of boron, lithium, or fluorine are optimal detector components. We give careful estimates of expected cross-sections and event rates and discuss optimal detector granularities.

1. Introduction

The rotation curves of spiral galaxies are flat out to large radii, indicating that galactic halos extend out far beyond the visible matter.[1] If this dark matter is non-baryonic, as suggested by a variety of arguments,[2] it may consist of one of several exotic candidates. Weakly interacting massive particles (WIMPs) are candidates in the GeV mass range which interact with ordinary matter with cross sections $\mathcal{O}(10^{-38})\,\mathrm{cm}^2$. WIMPs can be divided into two classes: (I) those with coherent interactions on matter, i.e., cross-sections $\propto N^2$, where N is approximately the atomic number of the scattering nucleus. Particles in this class include massive Dirac and scalar neutrinos and some solar cosmion candidates.[3] (II) Particles with spin-dependent interactions with matter, i.e., cross-sections proportional to nuclear spin. Particles in this class usually include photinos and Majorana neutrinos.[4]

Several astrophysical arguments as well as experiments at present already constrain the existence of WIMPs in certain mass ranges. The results from double β-decay experiments have been used to rule out a halo density of WIMPs of mass $\gtrsim 20$ GeV in Class I.[5] In addition, WIMPs in the halo could be captured in the Sun (if $m_W \gtrsim 3$ GeV) or in the Earth (class I only, if $m_W \gtrsim 12$ GeV); there they would sink to the core, and if there is no cosmic asymmetry, annihilate one another, giving rise to a potentially observable flux of ordinary massless neutrinos in proton decay detectors.[6] In this paper we will focus on WIMPs in class II, although we will briefly consider class I particles less massive than 20 GeV.

Recently there have been several proposals to build low temperature detectors of cold dark matter candidates from the halo of our Galaxy.[7–13] The goal of

these cryogenic detectors is to achieve sensitivity to energy deposits in the detector $\lesssim \mathcal{O}(\text{keV})$ due to elastic nuclear scattering of halo particles of mass $\gtrsim \mathcal{O}(\text{GeV})$. This new generation of detectors is required to detect particles of class II or low mass ($m_W \lesssim 8$ GeV) particles of class I. The designs that have been proposed include superconducting colloids, crystal bolometers, ballistic phonon detectors, and superfluid roton detectors.

In a previous paper,[11] Drukier, Freese, and Spergel discussed the WIMP signal from superheated superconducting colloid detectors (SSCD). The SSCD consists of a large number of small superconducting grains, and the signal due to a halo particle passing through the detector consists of a single grain flip from the superconducting to normal state. The SSCD is an example of a cryogenic detector in which the absorber (more precisely, the scatterer) and thermometer are physically identical.

In this paper we focus instead on the optimization of the signal from hybrid crystal bolometer detectors. In this case, energy deposition due to elastic scattering of WIMPs with nuclei in the detector also leads to a bulk temperature increase monitored electronically. In the crystal bolometer, however, the WIMP absorber is physically distinct from the thermometer. Diverse thermometers are being developed, e.g., doped semiconductor thermistors, superconducting junctions, and superconducting films. Thermometers with noise levels in the range $\delta T_n \simeq 10-100\,\mu K$ have been developed, and we assume thermometer performances in this range can be achieved in detectors. We turn therefore to a discussion of absorber materials.

Since the measured temperature increase is directly proportional to the energy deposited, crystal detectors operated in bolometric mode in principle have excellent

energy resolution. This is achieved, however, at some sacrifice of spatial resolution, which means that background rejection is a potential problem. As a result, one is forced to search for detector elements which yield the strongest signals. For particles in class II, the interaction cross-sections are generally low and depend strongly on the nuclear structure of the target. In particular, these particles couple very weakly with conventional detector elements such as germanium and silicon (which, in natural abundance, are composed primarily of even-even nuclei). Even with the alternative detector elements discussed below, the expected WIMP count rates are only of order a few events per kg per day,[11,14] comparable with expected radioactive backgrounds. Therefore we also consider the best choice of detector granularities and specific absorber compounds to optimize the signal.

In Section 2, we compare the expected event rates per unit mass for class II WIMPs in detectors of various materials. Among crystalline compounds, and taking into account expected radioactive backgrounds, this singles out ^{7}Li, ^{11}B and ^{19}F as having the best signal-to-noise ratios for moderate WIMP masses. In Section 3, we consider compounds of these 3 elements in more detail, using specific heat properties to optimize the choice of detector material. In Section 4, we discuss expected event rates and detector granularities and summarize our results in the Conclusion.

2. Signal Rates

To calculate the event rate in a detector, we need to know the WIMP cross-section and the kinematics of WIMP-nucleus scattering. We first discuss cross sections.

Cross-Sections

WIMP interaction cross-sections with matter (assumed to be isotropic and velocity independent) can be parametrized by[14]

$$\sigma = 2.1 \times 10^{-39} \frac{\mathrm{cm}^2}{\mathrm{GeV}^2} \frac{m^2 M^2}{(m+M)^2} Q^2 \tag{1}$$

where m, M are the WIMP and nuclear masses, and Q is a parameter which depends on the detector nucleus and the WIMP identity. For a discussion of relevant cross-sections and Q factors, see Appendix A. For class II particles, $Q^2 \propto \lambda^2 J(J+1)$, where J is the magnitude of the nuclear spin and λ is a nucleus-dependent shell model factor. Thus, class II particles effectively interact only with odd nuclei. In this case, the cross-section is optimized when the mass of the target nuclei is equal to the WIMP mass.

Energy Deposition

The energy lost by a WIMP of mass m with speed v in elastic scattering with a nucleus of mass M is

$$\Delta E = \frac{m^2 M}{(m+M)^2} v^2 (1 - \cos\theta) \tag{2}$$

where θ is the scattering angle. The maximum energy deposited by a WIMP

moving with the typical halo velocity $\overline{v}$ is thus

$$\begin{aligned} \langle E_{\max} \rangle &= \frac{2m^2 M}{(m+M)^2}\, \overline{v}^2 \\ &= 1.62\, \overline{v}_{270}^2 \left(\frac{m}{m+M}\right)^2 \left(\frac{M}{\mathrm{GeV}}\right)\ \mathrm{keV} \end{aligned} \tag{3}$$

where the halo velocity dispersion $\overline{v} = 270 \pm 25 \equiv 270\ \overline{v}_{270}$ km/sec. The fractional energy loss is maximized when the WIMP and nuclear masses are matched. For WIMPs of mass 5, 10, and 20 GeV, we show the maximum energy deposit $\langle E_{\max} \rangle$ for several detectors in Table 1. We note that in order to detect a significant fraction of the WIMPs in the halo, we require that the threshold energy E_{th} of the detector not be large compared to the maximum energy loss of typical WIMPs, $\langle E_{\max} \rangle$.

Event Rate

Using an isothermal model of the WIMP halo, the event rate per kg of detector can be shown to be[11,14]

$$\frac{R}{\mathrm{kg-day}} = 2.61 \left(\frac{2}{3\pi}\right)^{1/2} \left(\frac{\sigma}{A}\right) \left(\frac{6 \times 10^{26}}{\mathrm{kg}}\right) n_W \overline{v} \gamma(x) r \tag{4}$$

where A is the molecular mass of the detector, r is the number of atoms per detector molecule which have appreciable WIMP cross-section, n_W is the local number density of WIMPs of mass m, and the halo density is $\rho_{\mathrm{halo}} = n_W m \simeq 0.4\ \mathrm{GeV/cm^3}$ (to within a factor of 2). (The isothermal halo model yields the observed flat rotation curve at large radii.) The parameter $x \equiv 3E_{\mathrm{th}}/2\,\langle E_{\max} \rangle$, and the function $\gamma(x)$ is the signal at energy threshold E_{th} as a fraction of its value at zero threshold. Thus, $\gamma(0) = 1$ and $\gamma(x)$ falls monotonically with increasing x. [See Fig. 1.] For

fixed halo properties ($\rho_{\rm halo}, \overline{v}$) we see that the detection rate per kg per day scales as $R \propto (\sigma/Am)$. In this section, we focus on simple atomic (as opposed to molecular) detector elements, in which case A is the atomic mass and $r = 1$. Using Eq. (1), we can write Eq. (4) as

$$\frac{R}{\rm kg-day} = 1.3 \, \frac{mM}{(m+M)^2} \, Q^2 \gamma(x) \overline{v}_{270} \rho_{0.4} \tag{5}$$

where the halo density $\rho_{\rm halo} = 0.4 \ \rho_{0.4}$ GeV/cm^3. Using the results of Appendix A, this leads us to define our first figure of merit for detection of class II particles

$$FM_1 = 26.7 \, \frac{mM}{(m+M)^2} \, \lambda^2 J(J+1) \, f_{\rm odd} \ , \tag{6}$$

where $f_{\rm odd}$ is the fraction of the naturally occurring element with an odd number of neutrons or protons. (Recall class II particles do not scatter with even-even nuclei.) We have chosen to normalize FM_1 so that Eq. (6) gives the detection rate per kg per day for Majorana neutrinos at zero threshold (assuming the naive quark model–see Appendix A). The relevant nuclear data are shown in Table 2, and we give $\rm FM_1$ for several WIMP masses in Table 3, for a variety of detector elements.

Equation (6) gives a reliable figure of merit by which to compare different elements for detecting higgsinos and Majorana neutrinos. However, from Eq. A.5, we see that there is an extra factor entering the definition of Q^2 for photinos, which depends on whether the nucleus is "proton-like" or "neutron-like". This factor, in turn, depends on the poorly measured axial isosinglet coupling constant G_{A0}. For photinos, we therefore define the figure of merit

$$FM_{\tilde{\gamma}} = \frac{FM_1}{0.174} \left(\frac{5}{9} G_{A0} \pm \frac{1.25}{3} \right)^2 \tag{7}$$

where the $+(-)$ sign is for protonic (neutronic) shells. The coupling G_{A0} probably

lies in the range $0 \lesssim G_{A0} \lesssim 0.45$. The photino figure of merit is normalized so that, for $G_{A0} \simeq 0$, as suggested by recent EMC data, $FM_{\tilde{\gamma}} = FM_1$. We therefore show $FM_{\tilde{\gamma}}$ in Table 4 for the value $G_{A0} = 0.45$ to illustrate the range of possibilities, wherein $(FM_{\tilde{\gamma}}/FM_1) = 0.16$ and 2.55 for neutronic and protonic shells, respectively. For non-zero values of G_{A0}, 'protonic' materials are favored over 'neutronic' detectors for photino detection. (Note that $FM_{\tilde{\gamma}}$ does *not* give the normalized absolute photino rate.)

Tables 2-4 indicate that class II particle detection with conventional semiconducting detectors is unlikely. The detection rates for both Si and Ge are very low, well below 1 per kg per day, because they are both predominantly even nuclei, $f_{odd} \ll 1$. On the other hand, as Table 3 shows, these materials would become attractive if large samples enriched with the odd nuclei could be produced. Three superconducting materials $A\ell$, V and Ga have reasonable figures of merit, but $A\ell$ has a long lived radioactive isotope $A\ell^{26}$ which contributes a large background rate. The type I superconductors V and Ga appear promising, and have been discussed elsewhere.[10,11]

For non-superconducting crystals, it is apparent from Tables 2-4 that boron, lithium and fluorine are good candidates for class II detectors. From Table 3, we expect event rates in these materials up to a few per kg per day. We discuss the properties of these 3 detector materials in more detail in the next section.

3. Lithium, Boron, and Fluorine Detectors

3.1. Detector Optimization

In the discussion above, we selected detector materials from the standpoint of obtaining the largest count-rate per unit mass of detector. For crystal bolometers, there are additional factors to take into account in choosing materials. Since each channel of electronics used to detect a signal adds to the cost of the experiment and introduces heat into the detector system, it is advantageous to minimize the number of channels per detector mass. Thus, to attain the optimum signal, we seek to maximize the product

$$\frac{\text{Detection Rate}}{\text{electronic channel}} = \left(\frac{\text{Rate}}{\text{kg}}\right) \times \left(\frac{\text{kg}}{\text{channel}}\right) . \tag{8}$$

The first term on the right-hand side of Eq. (8) has been discussed above, and is embodied in the quantity FM_1. We show below that the second factor, the maximum mass per channel, is a function of the WIMP energy deposition and the material specific heat.

The energy resolution of the detector is limited by thermal fluctuations (phonon noise) in the absorber, Johnson noise in the thermometer, and Johnson noise due to the amplifier. We assume that the amplifier noise can be made subdominant by suitable design. Then the thermal energy fluctuation gives rise to an uncertainty in the energy of[12] $\delta E_{rms} = \xi(kT^2 C_v M_{det})^{1/2}$, where T is the operating temperature, C_v is the specific heat per unit mass of the absorber, M_{det} is the mass per channel, and ξ takes into account thermometer response (thermistors with $\xi \simeq 2$ have

been achieved). If this thermal limit could be achieved, then δE_{rms} would set the minimum resolution for a detector of mass M_{det} monitored by a single channel of electronics. This assumes, however, that thermistor response can be extrapolated down to arbitrarily small temperature increments. To be more conservative, we shall instead suppose the thermometer has a limiting intrinsic noise δT_n. Then, requiring a signal to noise ratio of, say, $S/N > 10$, the minimum "detectable" temperature increase is of order $\Delta T_{\rm min} \simeq 10\,\delta T_n$. Since an energy deposition ΔE leads to a temperature increase $\Delta T = \Delta E/C_v M_{det}$, the effective threshold for a detector of mass $M_{\rm det}$ monitored by a single channel of electronics is at least $E_{\rm th} \simeq 10\,\delta T_n M_{\rm det} C_v$. For large detectors operating at millikelvin temperatures, assuming $\delta T_n \geq \mathcal{O}(10\mu K)$, one generally finds $E_{th} >> \delta E_{rms}$, *i.e.*, the detector sensitivity is bounded by the thermometer response.

Clearly, increasing the detector mass per channel drives up the threshold energy, reducing the fraction of incident WIMPs detected. From Fig. 1, to have an appreciable signal, say $\gamma(x) \gtrsim 0.3$, requires $x \lesssim 2$, or $E_{\rm th} \lesssim \frac{4}{3}\langle E_{\rm max}\rangle$. Thus the maximum detector mass per channel is, using Eq. (3),

$$\left(\frac{M_{\rm det}}{\rm channel}\right)_{\rm max} \simeq \frac{2\langle E_{\rm max}\rangle}{15\,C_v \delta T_n} \propto \frac{m^2 M}{(m+M)^2 C_v}\,, \tag{9}$$

for given thermometer noise.

In crystals the specific heat is dominated by the lattice contribution, given by[15]

$$C_v(T) = \left(\frac{1.21\times 10^{19}}{A}\right) \times \left(\frac{T}{\theta_D}\right)^3 \left[\frac{\rm keV}{^\circ K - {\rm gm}}\right], \tag{10}$$

where A is the mass number of the detector molecule. This expression arises from assuming that C_v is simply proportional to the total number of molecules in the

crystal.[15] In fact, this assumption scales out of our results and only serves as a formal way to normalize the definition of the Debye temperature θ_D. That is, we use measured specific heats to infer the quantity $A\theta_D^3$, and it is this factor which enters the expressions below. Since $C_v \propto \theta_D^{-3}$, we seek materials with large Debye temperatures. The relevant thermodynamic data are provided in Tables 5 and 6 for selected boron, lithium, and fluorine compounds.

Combining Eqs. (6)-(10), we define a new figure of merit for optimizing the rate per electronics channel for class II WIMPs,

$$FM_{el} = \frac{m^3 M^3 \lambda^2 J(J+1)}{(m+M)^4} f_{\rm odd}\, \theta_D^3 r_{eff} \tag{11}$$

(with an appropriate additional multiplicative factor $\propto (0.56\ G_{A0} \pm 0.42)^2$ for photinos). This is shown in Table 7 for B, $F\ell$, and Li compounds. In Eq. (11), for compound molecular detectors, we are only including scattering from the nuclei (i.e., B, F, or Li) with the largest cross-sections for class II WIMPs. Here, M refers to the mass of this most 'active' scattering atom, while θ_D is the Debye temperature of the detector compound. Also, r_{eff} is the number of 'active' atoms per detector molecule (e.g., $r = 4$ for XeF_4). For detectors with multiple 'active' nuclei, e.g., $LiHF_2$, the entries in Table 7 underestimate the figure of merit by less than a factor of two. Such detector elements would potentially give rise to a distinctive WIMP signal, since each nucleus will have a different recoil spectrum.

Boron crystals of very high purity (a few parts in 10^9) have been grown, and their Debye temperature is very high, $\theta_D(B) \approx 1480°K$. Thus a crystal of boron with a mass of 100 grams has specific heat $C = 3.4 \times 10^4$ keV/$°K$ at $T = 10\ mK$.

For WIMPs with $m = 5$ GeV, the typical energy transfer is $\langle E_{\max} \rangle / 2 = 0.9$ keV. Thus $\Delta T \simeq 27$ microkelvin heating is expected, which should be detectable with thermistors. Note that, in this case, the rms phonon noise is negligible, $\delta E_{rms} \simeq 1$ eV. Alternatively, boron nitride might be used, $\theta_D(BN) = 780°K$.

Lithium is a non-superconducting metal, and has a large electronic specific heat ($\sim T$) even at very low temperatures. However, LiF will have almost as large a cross section as pure Lithium. Big crystals of LiF have been grown which possess an adequately high Debye temperature, $\theta_D(LiF) \approx 570°K$. The Debye temperature of lithium hydride is even more favorable, $\theta_D(LiH) \approx 619°K$. Unfortunately, lithium has chemical properties similar to potassium, so that lithium based detectors may be contaminated with K^{40}. This may favor boron based detectors over those using lithium compounds. (See Appendix B for a brief discussion of radioactive backgrounds.)

Detectors based on boron and lithium may have a radioactive background due to absorption of neutrons. Naturally occurring lithium and boron contain isotopes which strongly absorb neutrons: Li^6(7.4%, $\sigma = 950$ barn) and B^{10}(18.7%, $\sigma = 3836$ barn). Fortunately, the neutron induced reactions deposit much more energy than the scattering of weakly interacting particles, so that some rejection based on heat pulse height analysis is possible, but the use of isotopically enriched materials may be necessary. These are available commercially.

Fluorine compounds can also be used as class II WIMP detectors. Some of the fluor salts are available in crystalline form (see Table 6). The case of LiF was already discussed; the other crystals with reasonably high Debye temperature are $MgF_2(\theta_D = 364°K)$, $NaF(\theta_D = 353°K)$, $AlF_3(\theta_D = 343°K)$, $CaF_2(\theta_D =$

$334°K$). Two of these have long life isotopes producing backgrounds of 2.18×10^5 counts/kg/day for $A\ell F_3$, and 70 counts/kg/day for CaF_2. This leaves MgF_2, LiF and NaF as good candidates for class II detection (although, due to chemical affinity, NaF would have to be checked for contamination with K^{40}).

We point out that candidates for "cosmions", particles which may solve the solar neutrino problem,[3] include Majorana fermions, i.e., class II particles. For these particles, the result is the same: boron appears to be the most suitable detector. However, the expected count rates are much larger for these Majorana type solar cosmions than for the previously discussed class II candidates, since they must have large scattering cross-sections in the sun. A single 100g boron crystal operating at $T = 10$ mK will produce hundreds of counts/day when used as a solar Majorana cosmion detector.

For completeness, we mention that for particles of class I, such as scalar or Dirac neutrinos, the event rate increases monotonically with the mass of the detector nucleus (see Appendix A.1). Thus heavier detector elements are preferred.[8–14].

So far, we have assumed an ideal detector obeying the Debye model; to apply our discussion to realistic detectors, we must issue several caveats. First, it should be pointed out that the thermodynamic properties of diverse compounds are based on low, but not very low, temperature measurements (see Ref. 15). Generally, the density of vibrational states can be written as $F(w) = a_1 w^2 + a_2 w^4 + \ldots$, where the Debye approximation corresponds to keeping only the first term in the series. In the low-temperature limit, the term proportional to a_2 gives rise to a contribution $\propto T^5$ in the heat capacity. This can be incorporated into the Debye model as a

temperature-dependent Debye temperature[15]

$$\theta_D(T) = \theta_D(0)\left[1 - \left(\frac{20\pi^2}{21}\right)\left(\frac{a_2}{a_1}\right)\left(\frac{kT}{\hbar^2}\right)^2\right] . \qquad (12)$$

For almost all solids, the coefficient $a_2 > 0$. Thus, as the temperature is lowered below about $\theta_D(\infty)/5$, $\theta_D(T)$ typically passes through a minimum and, at very low temperature, increases according to Eqn.(12) as $T \to 0$. The very-low temperature value $\theta(0)$ is reached at temperatures of order $\theta_D(\infty)/100$ (where $\theta_D(\infty)$ is the Debye temperature measured at high temperatures, $T \sim \theta_D$). Thus, at the operating temperatures of interest, say, $T \simeq 0.01°K$, the actual Debye temperature may be up to 50% higher than the values quoted in Tables 5 and 6. [For example, in Si, $\theta_D(0) \simeq 640°K$ and drops to a minimum of $\theta_D(40°K) \simeq 470°K$.] As a result, the count rates based on the data in Tables 5 and 6 are likely to be lower bounds to the actual rates.

Furthermore, at very low temperatures ($T \lesssim 0.01\theta_D$), processes other than lattice vibrations can contribute significantly to the specific heat. In crystals, these effects may include chemical and isotopic impurities and other defects, nuclear spins, and surface effects in very small samples.[15] For example, consider a mass defect: if the mass of some atoms in the lattice is changed from M to M', the Debye temperature is changed to[15]

$$\theta_D(c) = \theta_D(0)\left[1 - c\left(1 - \frac{M'}{M}\right)\right]^{-1/2} , \qquad (13)$$

where $c = N'/N$ is the impurity concentration (N is the number of atoms of mass M in the detector). Thus, for heavy defects ($M' > M$), the sample must be made

sufficiently pure to avoid degrading the Debye temperature. In addition, for heavy impurities, there is a contribution to C_v from the $3Nc$ resonance modes[15] which is peaked at very low $T \ll \theta_D$. (For example, in silicon, the specific heat due to impurities peaks around $T \simeq 20\ mK$.) Additional experimental studies of the very low temperature specific heats for selected compounds (e.g., B, BN, LiH, LiF, NaF and MgF_2) are a necessary prerequisite for the future development of class II WIMP detectors.

Finally, we have implicitly assumed that all of the deposited energy is converted into phonons which are rapidly thermalized (*i.e.*, on a timescale of milliseconds). In some cases, however, a significant fraction of the phonons may remain ballistic (with energies of order meV) over a longer timescale. (Of course, this is not a problem if the ballistic phonons themselves can be detected.[12]) In addition, in Si detectors, it has been estimated[12] that, above a few keV, up to 30% of the deposited energy (from x-rays) goes instead into electron-hole pairs produced by ionization. Some of the produced electrons may be lost due to trapping by impurities and defects before they can recombine. Due to these losses, the true detector threshold is higher than in the ideal detector.

3.2. Event Rates and Granularity

In the previous section, we discussed the figure of merit for various crystal bolometers; here we illustrate expected count rates for a boron detector.

The detector mass one can instrument with one channel of electronics is given

by

$$M_{\rm det} = \frac{E_{\rm th}}{C_v \Delta T_{\rm min}} \ . \tag{14}$$

Since we would like a signal-to-noise ratio of at least 10, and thermometers with noise less than of order $\delta T_n \simeq 50\ \mu K$ have been developed, we will take $\Delta T_{\rm min} \simeq 0.5$ mK. Thus, the maximum mass per channel for a boron detector is, from Table 5,

$$M_{\rm det} = 5.9\ {\rm kg} \left(\frac{E_{\rm th}}{\rm keV}\right) \left(\frac{T}{10^{-3} K}\right)^{-3} \left(\frac{\Delta T_{\rm min}}{0.5\, mK}\right)^{-1} \tag{15}$$

where T is the operating temperature of the detector. Equation (15) shows that the detector mass is a sensitive function of the operating temperature and, to a lesser extent, of the thermal noise. Thus, for an operating temperature of order $T \simeq 1\, mK$, and $\Delta T_{\rm min} \simeq 1/2\, mK$, the detector could in principle be monitored by a single channel of electronics. We believe, however, that to reach $1 mK$ is too difficult experimentally. Modern commercial dilution refrigerators can operate with good stability down to $T \simeq 10\, mK$, and perhaps as low as 5 mK. (These cryostats have a temperature stability better than $\Delta T \lesssim 10\, \mu K$, so the sensitivity is expected to be limited by the thermometer.)

As an example, we consider a Majorana neutrino of mass $m = 5$ GeV. From Table 1 and Eqs. (5) and (15), given N_c electronics channels and a minimum desired rate of $R_{\rm min}$ total counts per day, the operating temperature must be less than

$$\left(\frac{T}{mK}\right)^3 \left(\frac{\Delta T_{\rm min}}{0.5\, mK}\right) < 14 \left(\frac{E_{\rm th}}{\rm keV}\right) \frac{N_c}{R_{\rm min}} \overline{v}_{270} \rho_{0.4} \gamma(E_{\rm th}/1.2\,{\rm keV}) \ . \tag{16}$$

For presently existing resistivity thermometers such as thermistors, one needs 4 wires per channel. Suppose that, in order to keep down thermal noise, one wants

to use no more than $\simeq$ 100 wires, i.e., $N_c \lesssim 25$ channels. Thus, we would require a mass per channel $M_{\rm det} \gtrsim$ 40-80 gm to obtain a reasonable count rate. For example, for 5 GeV Majorana neutrinos, for energy threshold in the range $E_{\rm th}$ = 1-3 keV, for 25 channels of electronics and $\Delta T_{\rm min} = 0.5\,mK$, from Eq. (16) we find $T \leq 6\,mK$ to obtain $R_{\rm min} > 1$ count per day. For some materials, this temperature requirement may be a limiting factor: as we noted above, in some cases the specific heat may be dominated by impurities, rather than the lattice modes, over a range of ultra-low temperatures. If the contribution from impurities peaks at sufficiently low temperature, it may only be feasible to operate the detector at higher temperature. For example, suppose the minimum operating temperature is $T \simeq 20\,mK$ for a boron detector of 5 GeV halo Majorana neutrinos. In this case, to achieve of order 1 count per day would require many hundreds of channels, each monitoring a segment of mass $M_{\rm det} \simeq 1$ gm. Implementing such an excessive number of channels appears infeasible.

4. Conclusions

We have analyzed several candidate cryogenic detectors of massive weakly interacting dark matter particles. The detection of coherently interacting particles (class I), e.g., massive Dirac neutrinos and supersymmetric neutrinos, is well within the state of the art of crystal bolometers. Detection of particles with spin dependent interactions is a difficult experimental challenge but not impossible. We believe that the main experimental obstacle is attaining the required ultralow radioactive background; the sensitivity of bolometers is adequate if the ultra-low temperature behavior of crystals approximates the Debye law. Furthermore, we have shown

that the appropriate choice of material can significantly improve the signal-to-noise level in the case of class II WIMP detection. Unfortunately, at the very low required operating temperatures ($T \ll 1°K$), specific heats of the appropriate materials are often not known. A strong experimental effort will be required to create the "data bank" of very low temperature properties of materials to be used as cryogenic particle/radiation detectors.

We conclude by outlining the main points of our discussion. To optimize the total event rate per kg for class II WIMP detection, given by FM_1 and its variants, we are led to boron, lithium and fluorine as primary absorber components. Consideration of specific heat properties then shows that the maximum rates per electronics channel are achieved for the compounds B, BN, LiF, LiH, NaF, and MgF_2. Further work on the radioactive backgrounds in, and ultralow temperature behavior of these compounds will be required to see which of these can be made into efficient WIMP detectors. We note that the rate per kg, $R/\text{kg} \propto \gamma(x)$, is clearly maximized at zero energy threshold, $x = 0$ (the 'dark matter peak'). However, as Eqn.(13) shows, the rate per channel is proportional to the product $x\gamma(x)$, which reaches a maximum at $x \simeq 2$. In general, a compromise value of the energy threshold must be chosen to satisfy the simultaneous constraints that the total detector mass, $M_{det} \simeq 1 - 2$ kg, can be instrumented with a moderate number of electronics channels, at threshold low enough to achieve $R_{min} \geq \mathcal{O}(1)$ count per day. For the most favorable detector compounds, these constraints can be satisfied for class II WIMPs with thresholds $E_{th} \sim 1$ keV, if sufficiently low operating temperatures, $T \lesssim 5 - 10\ mK$, can be achieved.

Acknowledgements:

A. D. would like to thank J. Bahcall and D. Spergel for their warm hospitality at the Institute for Advanced Studies, and thanks F. Avignone, G. Gelmini, M. LeGros, R. Harms, S. Murray and especially A. Kotlicki for enlightening discussions. J. F. thanks Blas Cabrera for helpful discussions.

- APPENDIX A

As mentioned in the Introduction, WIMPs can be classified according to whether their interactions with nuclei are: I) coherent, i.e., nuclear spin-independent, or II) spin-dependent. We will discuss examples of each type.

A.1. Coherent Particles

For particles with spin-independent interactions, Q is roughly proportional to the atomic number of the nucleus, i.e., to the nuclear mass. For example, for Dirac neutrinos elastically scattering from a nucleus with N neutrons and Z protons, the cross-section is

$$\sigma_{\nu_D} = \frac{G_F^2}{8\pi}\left(\frac{mM}{m+M}\right)^2 [N - (1 - 4\sin^2\theta_w)Z]^2 \ , \tag{A.1}$$

where G_F is the Fermi constant. From Eqn. 1, this gives

$$Q_{\nu_D} = N - (1 - 4\sin^2\theta_w)Z \simeq N - 0.12\,Z \ , \tag{A.2}$$

slightly less than the number of neutrons. (We are ignoring the small contribution due to the axial vector coupling, which is negligible for $Z \gtrsim 2$.) For scalar neutrinos, candidates for the lightest supersymmetric particle, $Q_{\tilde{\nu}} = 2Q_{\nu_D}$.

A.2. Spin-Dependent Interactions

Popular candidates for halo particles with spin-dependent nuclear interaction include three Majorana fermions: Majorana neutrinos, higgsinos and photinos. For Majorana neutrinos,[6,14]

$$Q^2_{\nu_M} = 13.2 g^2_{A(p,n)} \lambda^2 J(J+1) f_{odd} \ , \tag{A.3}$$

where $\lambda^2 J(J+1)$ is a parameter which depends on the nucleus, and f_{odd} is the fraction of the element with odd nuclei. J is the magnitude of the nuclear spin and λ is a parameter which, in the nuclear shell model, is given by

$$\lambda = 0.55 \left(1 + \left[\frac{s(s+1) - \ell(\ell+1)}{j(j+1)}\right]\right) ,$$

where s, ℓ and j are the spin, orbital and total angular momenta of the extra proton, neutron, or proton (neutron) holes. Here and below, we have normalized our definitions of Q^2 so that the values of $\lambda^2 J(J+1)$ given by Goodman and Witten (Ref. 8) and Drukier, Freese and Spergel (Ref. 11) should be used, even in cases where our estimates for cross sections differ. The nuclear shell model parameter $\lambda^2 J(J+1)$ is only appreciable for nuclei with an odd number of protons or neutrons (see Table 2). In (A.3), the axial coupling constant g_A is that of the extra proton or neutron (holes). This constant is not well-determined experimentally. In the naive quark model, $g_{Ap} = g_{An} = 1.25$; these values have been used in arriving at Eqn. 6. Recently, however, the spin-dependent structure function of the proton was measured by the EMC collaboration[16] at $q^2 = 3$ GeV^2, giving a value approximately half of that predicted by the quark model. If we assume the structure function

does not have strong dependence on q^2, this may be interpreted[17] as implying the values $g_{Ap} = 1.5$, $g_{An} = 1.0$. If these values are accepted, the figure of merit FM_1 in Table 3 should be multiplied by a factor 2.2 for elements with an extra proton (or proton hole) and by 0.8 for elements with an extra neutron (or neutron hole). Aside from shell model factors, this would somewhat favor 'protonic' detectors for Majorana neutrinos.

In supersymmetric theories, the lightest supersymmetric particle LSP may be a Majorana fermion, a partner to ordinary bosons. In general, the lowest mass eigenstate will be a mixture of the photino, higgsinos, and the zino. We will consider two limiting cases, in which the LSP is an almost pure higgsino or an almost pure photino. For higgsinos,[6]

$$Q^2_{\tilde{H}} = Q^2_{\nu_M} \cos^2 2\alpha \ , \tag{A.4}$$

where $\tan\alpha = v_1/v_2$ is the ratio of the vacuum expectation values of the two Higgs doublets. The result of Eq. (A.3) assumes higgsinos scatter predominantly through Z_0 (rather than squark) exchange, which holds provided α is not too close to $\pi/4$, i.e., for $\tan\alpha \neq 1$. Theoretical prejudice appears to favor $\tan\alpha < 1$.

For photinos, the nuclear scattering cross-sections are somewhat uncertain, since they depend more severely on the spin content of the nucleon. Assuming all scalar quark masses $m_{\tilde{q}}$ are degenerate and negligible left-right squark mixing, the photino-nucleus cross section can be written[14]

$$Q^2_{\tilde{\gamma}} = 271.5 \left(\frac{50\,\mathrm{GeV}}{m_{\tilde{q}}}\right)^4 \lambda^2 J(J+1) f_{odd} \left[\frac{1}{2}\left(\frac{5}{9} G_{A0} \pm \frac{1.25}{3}\right)\right]^2 \ , \tag{A.5}$$

where the $+(-)$ sign is for nuclear shells with an extra proton (neutron) or proton

(neutron) hole. The isosinglet coupling G_{A0} is not well determined experimentally, so we retain it as a parameter. In this expression, we have scaled the cross-section to that for a scalar quark mass of 50 GeV, the lower limit set by UA1 data.[18] (This limit may now be as high as 70–80 GeV from Tevatron data.)[19]

If we further assume degeneracy between the lightest squark and slepton masses, a "Lee-Weinberg" calculation implies an approximate relation between squark and photino masses[6] (for $m_{\tilde{\gamma}} \gtrsim 10$ GeV)

$$m_{\tilde{q}} = 56\,\mathrm{GeV}\,(1 + 0.04\,m_{\tilde{\gamma}}^2)^{1/4} \left(\frac{\Omega_{\tilde{\gamma}} h^2}{0.25}\right)^{1/4} , \qquad \text{(A.6)}$$

where $m_{\tilde{\gamma}}$ is the photino mass in GeV, $h = H_0/100\,\mathrm{km\,sec^{-1}\,Mpc^{-1}}$ is a measure of the Hubble constant, and we have approximately scaled the results from the case $\Omega_{\tilde{\gamma}} h^2 = 1/4$ treated in Ref. 6. Given these assumptions, we can express the photino scattering parameter as

$$Q_{\tilde{\gamma}}^2 = \frac{43.2\lambda^2 J(J+1) f_{odd}}{(1 + 0.04\,m_{\tilde{\gamma}}^2)} \left(\frac{\Omega_{\tilde{\gamma}} h^2}{0.25}\right)^{-1} \left(\frac{5}{9} G_{A0} \pm 0.417\right)^2 . \qquad \text{(A.7)}$$

Different values for the axial isosinglet coupling G_{A0} have been used in the literature. Goodman and Witten[8] use the quark model prediction $G_{A0} = 1$, while Srednicki, Olive and Silk[6] use the quark model relation $G_{A0} = 0.75$; Kane and Kani[20] use SU(3) flavor relations to obtain $G_{A0} = 0.45$. Although these values give differing cross sections, they all imply that nuclei with an extra proton are favored over those with an extra neutron for photino detection. On the other hand, the recent EMC data imply a much smaller value for the isosinglet coupling, $G_{A0} \simeq 0.01$. In this case, aside from shell model factors, nuclei with an extra proton or an extra neutron would be roughly equally favorable for photino detection.

APPENDIX B. Radioactive Background

It is expected that the major source of background will be radioactive contamination of the detector and the cryostat. The typical contaminants are K^{40}, Uranium and Thorium. To detect class II WIMPs, purities better than a few parts per 10^9, and good background rejection, e.g., using spatial and energy resolution, are required. For example, materials based on elements with chemical affinity to potassium should be very carefully studied for K^{40} contamination.

It should be remembered that it is much easier to purify a detector chemically to a few parts in 10^9 than to perform isotopic selection on the level of a part in 10^{12} or better. Thus, materials with long-lived isotopes, e.g., C^{14}, $A\ell^{26}$ should be discarded as weakly interacting particle detectors. Table 9 shows the known long life radioactive isotopes and their abundance in the earth's crust.

Unfortunately, Aluminum has a radioactive isotope $A\ell^{26}$ and the expected radioactive background is about 6.8×10^5 counts/kg/day. It can be partially suppressed because $A\ell^{26}$ is a positron emitter, i.e., there will also be annihilation photons. However, the required anticoincidence detector would considerably complicate detector construction. Methods of radioactive background suppression when using superconducting colloids were described elsewhere (see Refs. 7 and 11).

Similarly, the existence of long life isotopes makes difficult the development of some otherwise promising crystal bolometers. The expected radioactive background in counts/kg/day is 2.1×10^{11} for berylia (Be_2O_3), 4.6×10^{11} for diamond, 3.6×10^5 for sapphire ($A\ell_2O_3$), and 5.8×10^5 for zirconia (ZrO_2).For the case of

short living radioisotopes, such as C^{14}, some improvement can be obtained by use of very old minerals, i.e., by using isotopically purified materials. At any rate, with the exception of sapphire, the above mentioned elements do not have large cross-sections for class II WIMP detectors.

Various methods of background rejection are discussed in Refs. 7, 10-14.

REFERENCES

1. S. M. Faber and J. S. Galligher, Ann. Rev. Astr. Astrophys. 17 (1979) 135; D. Burstein and V. C. Rubin, Astrophys. J297 (1985) 423; T. S. van Albada and R. Sancisi, "Dark matter in spiral galaxies", to be published in Phil. Trans. R. Soc. London, A (1986). For a General discussion, see "Dark matter in the Universe", Proc. of IAU Symposium 117, Princeton, June 1985, ed. J. Kormendy and G. R. Knapp (Reidel, Dordrecht, 1986).

2. D. Hegyi and K. A. Olive, in *Inner Space/Outer Space*, ed. by E. Kolb *et al.* (University of Chicago Press, 1986). J. R. Primack, in Proc. of Intl. School of Physics "Enrico Fermi", Varenna, Italy 1984.

3. D. Spergel, W. H. Press, Ap. J. 294 (1985) 663; W. H. Press, D. N. Spergel, Ap. J. 296 (1985) 679; J. Faulkner, R. Gilliland, Ap. J. 299 (1985) 663; L. M. Krauss, K. Freese, D. N. Spergel, W. H. Press, Ap. J. 299 (1985) 1001; G. B. Gelmini, L. J. Hall, M. J. Lin, Nucl. Phys. B281 (1987) 726; S. Raby and G. West, Nucl. Phys. B292 (1987) 793; Phys. Lett. 194B (1987) 557; 200B (1988) 547; 202B (1988) 47; G. Steigman, C. Sarazin, H. Quintana and J. Faulkner, Astron. J. 83 (1978) 1050.

4. See, however, K. Griest, Fermilab preprint (1988).

5. S. P. Ahlen, F. T. Avignone, R. L. Brodzinski, A. K. Drukier, G. Gelmini, D. N. Spergel, Phys. Lett. 195B, 603 (1987). D. O. Caldwell, in "Neutrino Masses and Neutrino Astrophysics", Proc. of Telemark IV Conference, eds. V. Barger et al. (World Scientific, 1987).

6. J. Silk, K. A. Olive and M. Srednicki, Phys. Rev. Lett. 55 (1985) 257. M. Srednicki, K. A. Olive and J. Silk, Nucl. Phys. B279 (1987) 804. L. Krauss, K. Freese, D. Spergel and W. Press, Astrophys. J. 299 (1985) 1001. K. Freese, Phys. Lett. 167B (1986) 295. L. Krauss, M. Srednicki and F. Wilczek, Phys. Rev. D33 (1986) 2079. T. Gaisser, G. Steigman and S. Tilav, Phys. Rev. D34 (1986) 2221. K. Greist and D. Seckel, Nucl. Phys. B283 (1987) 681. K. Ng, K. Olive and M. Srednicki, Phys. Lett. 188B (1987) 138. A. Gould, Astrophys. J. 321 (1987) 571. IMB collaboration preprint, 1986. Kamiokande collaboration preprint, 1987.

7. A. K. Drukier and L. Stodolsky, Phys. Rev. D30 (1984) 2296.

8. M. Goodman and E. Witten, Phys. Rev. D31 (1985) 3059.

9. I. Wasserman, Phys. Rev. D22, 2071 (1986).

10. A. K. Drukier, Acta Physica Polonica B17 (1986) 229.

11. A. K. Drukier, K. Freese and D. N. Spergel, Phys. Rev. D23 (1986) 3495.

12. H. H. Anderson, C. C. Mauke, H. Sorenson, Rev. Sci. Instr. 38 (1967) 511; T. O. Njinikoski, F. Udo, CERN Report No. 74 (1974) 6 (unpublished); A. K. Drukier and L. Stodolsky (1982) unpublished; E. Fiorini, T. O. Njinikski, Nucl. Instrum. Methods 224 (1984) 83; S. H. Moseley, J. C. Mather, D. McCammon, J. Appl. Phys. 56 (1984) 1257; D. McCammon, S. H. Moseley, J. C. Mather, R. F. Musotzky, J. Appl. Phys. 56 (1984) 1263; B. Cabrera, L. M. Krauss, F. Wilczek, Phys. Rev. Lett. 55 (1985) 25; H. H. Anderson, Nucl. Instrum. Methods B12 (1985) 437; B. Cabrera, D. Caldwell and B. Sadoulet, Proc. of 1986 Summer Study on Physics of the

SSC, Snowmass, CO, July 1986. C. J. Martoff, et al., in Second Conference on Intersections between Particle and Nuclear Physics, Lake Louise, Canada, May 1986, ed. by D. F. Geesaman (AIP Proc. New York, 1986, Vol. 150). R. E. Lanou, H. J. Maris, G. M. Seidel, Phys. Rev. Letts. 58 (1987) 2498.

13. For general reviews of dark matter detection, see P. F. Smith, preprint RAL-86-029, and J. Primack, D. Seckel and B. Sadoulet, UCSC preprint, to appear in Ann. Rev. Nucl. Part. Sci.

14. K. Freese, J. Frieman and A. Gould, Phys. Rev. D37 (1988) to appear.

15. J. M. Ziman, *Principles of the Theory of Solids*, (Cambridge University Press, 1972). G. Grumvall, *Thermophysical Properties of Materials*, (North-Holland, 1986). Y. S. Touloukien, E. M. Buyco, *Specific Heat*, (IFI/Plenum, New York, 1970). M. Blackman, in *Crystal Physics I*, vol. 7, p. 365, Handbuch der Physik (Heidelberg, 1955). G. A. Slack, *Solid State Physics*, vol. 34 (Academic Press, 1979).

16. EMC Collaboration, talk presented at Uppsala Conference, 1987.

17. J. Ellis, talk presented at Uppsala Conference, 1987.

18. C. J. Seez (UA1 Collaboration), talk presented at the 2nd Topical Seminar on Heavy Flavor Physics, San Miniato, Italy (May, 1987).

19. D. Cline, private communication.

20. G. Kane and I. Kani, Nucl. Phys. B277 (1986) 525.

FIGURE CAPTIONS

1) Dimensionless nuclear recoil spectrum for an isothermal halo model (Eqn. 4). The abscissa is a measure of the ratio of the energy threshold to the typical energy transfer from a halo WIMP.

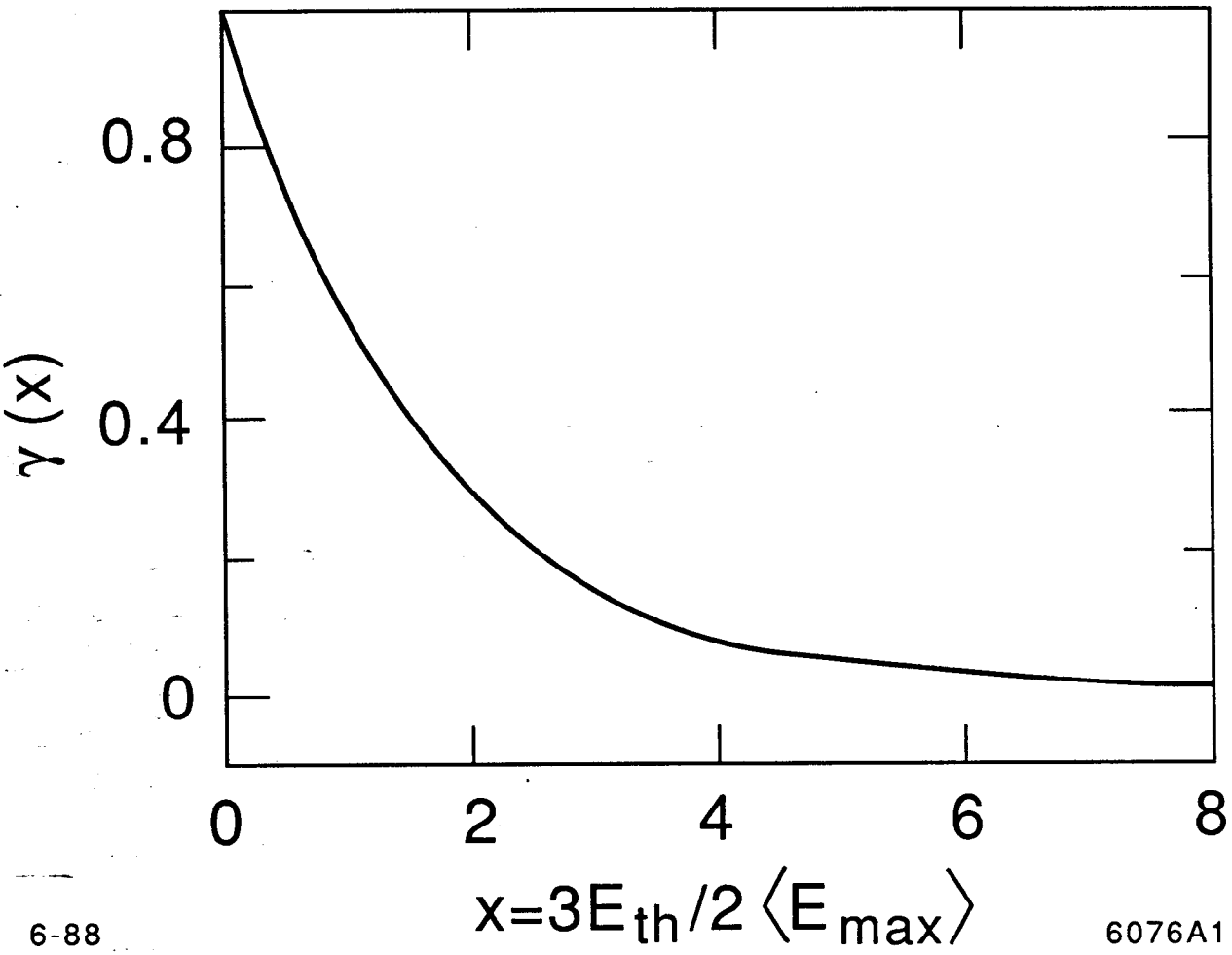

Fig. 1

Table 1

$\langle E_{\max} \rangle / \bar{v}_{270}$ for diverse detectors*

Element	$\langle E_{\max} \rangle$ /keV		
	$m = 5$ GeV	$m = 10$ GeV	$m = 20$ GeV
H	1.08	1.27	1.39
He^3	1.87	2.77	3.50
Li^7	1.99	3.87	6.02
Be^9	1.90	4.02	6.74
B^{11}	1.79	4.05	7.26
F^{19}	1.39	3.74	8.07
$A\ell^{27}$	1.12	3.30	8.00
Si^{29}	1.07	3.20	7.92
$C\ell^{35,37}$	0.93	2.19	7.64
V^{51}	0.70	2.33	6.76
$Ga^{69,71}$	0.56	1.93	5.96
Ge^{73}	0.52	1.81	5.69

* Halo velocity dispersion $\bar{v} = 270\ \bar{v}_{270}$ km sec^{-1}.

Table 2

Different Elements as Class II WIMP Detectors

Element	f_{odd}	$\lambda^2 J(J+1)$	Shell Model
H	1	0.91	
He^3	1.7×10^{-4}	0.91	$s^{1/2}$ neutron-hole (good)
Li^7	0.93	0.50	$p^{3/2}$ proton (good)
Be^9	1	0.50	$p^{3/2}$ neutron-hole (good)
B^{11}	0.80	0.50	$p^{3/2}$ proton-hole (good)
F^{19}	1	0.91	$s^{1/2}$ proton (good)
Al^{27}	1	0.42	$d^{5/2}$ proton-hole (good)
Si^{29}	0.047	0.91	$s^{1/2}$ neutron-hole (good)
$Cl^{35,37}$	1	0.18	$d^{3/2}$ proton
V^{51}	0.99	0.40	$f^{7/2}$ proton-hole (good)
$Ga^{69,71}$	1	0.50	$p^{3/2}$ proton (fair)
Ge^{73}	0.078	0.37	$g^{9/2}$ neutron (good)

Table 3

Figure of Merit for Class II WIMP Detectors*

Element	FM_1		
	$m = 5\ GeV$	$m = 10\ GeV$	$m = 20\ GeV$
He^3	9.5×10^{-4}	6.9×10^{-4}	4.4×10^{-4}
$^{\dagger}He^3$ (pure)	5.59	4.15	2.61
Li^7	3.05	2.97	2.31
Be^9	3.13	3.31	2.78
B^{11}	2.35	2.67	2.39
F^{19}	4.17	5.60	6.05
$A\ell^{27}$	1.55	2.28	2.77
Si^{29}	0.15	0.23	0.28
$^{\dagger}Si^{29}$ (pure)	3.19	4.89	5.96
$C\ell^{35,37}$	0.55	0.86	1.13
V^{51}	0.91	1.54	2.23
$Ga^{69,71}$	0.89	1.56	2.42
Ge^{73}	0.049	0.086	0.135
$^{\dagger}Ge^{73}$ (pure)	0.63	1.10	1.73

* Rate per kg per day for Majorana neutrino detection at zero threshold, assuming naive quark model couplings. For couplings inferred from EMC data (see Appendix A), the entries for the 'neutronic' elements (He^3, Be^9, Si^{29}, Ge^{73}) should be multiplied by 0.8, and all others by 2.2.

† Enriched element ($f_{\text{odd}} = 1$).

Table 4

Figure of Merit for Photino Detectors*

Element	$FM_{\tilde{\gamma}}$		
	$m = 5\ GeV$	$m = 10\ GeV$	$m = 20\ GeV$
He^3	1.5×10^{-4}	1.1×10^{-4}	7.1×10^{-5}
He^3 (pure)	0.89	0.66	0.42
Li^7	7.78	7.57	5.89
Be^9	0.50	0.53	0.44
B^{11}	6.0	6.81	6.09
F^{19}	10.63	14.31	15.43
$A\ell^{27}$	3.95	5.81	7.06
Si^{29}	0.024	0.036	0.044
$C\ell^{35,37}$	1.40	2.20	2.89
V^{51}	2.35	3.93	5.69
$Ga^{69,71}$	2.27	3.98	6.17
Ge^{73}	7.8×10^{-3}	0.014	0.022

* Assuming axial isosinglet coupling from $SU(3)$ flavor relations, $G_{A0} = 0.45$ (see Appendix A). For the EMC data, $G_{A0} \simeq 0$, the entries in Table 4 reduce to those in Table 3. Note that $FM_{\tilde{\gamma}}$ does *not* give the normalized absolute photino detection rate.

Table 5

Boron and Lithium Compounds as Class II WIMP Detectors*

	A	$\theta_D(^\circ K)$	$T_{\rm meas}(^\circ K)$	$C_v(10\ mK)^a$
B	11	1480	4.2	340
BN	25	780	4.2	10^3

	A	$\theta_D(^\circ K)$	$T_{\rm meas}(^\circ K)$	$C_v(10\ mK)^a$
LiH	8	619	3.72	6.4×10^3
LiF	26	570	2.31	2.5×10^3
Li_20	30	488	17.06	3.5×10^3
$LiCl$	42	321	13.77	8.7×10^3
$LiHF_2$	46	254	6.57	1.6×10^4

* Debye temperatures were obtained from Refs.13, using specific heats at the lowest measured temperatures $T_{\rm meas}$.

a Specific heat at $T = 10\ mK$. Units are keV $\mathrm{gm}^{-1}\ {}^\circ K^{-1}$.

Table 6

Fluorine and Its Compounds as Class II WIMP Detectors*

	A	$\theta_D(^\circ K)$	$T_{\rm meas}(^\circ K)$	$C_v(10\ mK)^a$
MgF_2	62	364	54.22	4.1×10^3
NaF	42	353	54.01	6.6×10^3
AlF_3	84	343	53.65	3.6×10^3
CaF_2	78	334	53.51	4.2×10^3
ZnF_2	103	267	11.03	6.2×10^3
VF_3	108	256	54.89	6.7×10^3
NiF_2	97	244	11.14	8.6×10^3
FeF_2	94	240	11.33	9.3×10^3
BeF_2	47	230	7.90	2.1×10^4
NbF_5	188	198	52.40	8.3×10^3
CoF_2	97	196	10.73	1.7×10^4
BaF_2	175	170	13.79	1.4×10^4
MnF_2	93	133	13.18	5.5×10^4
XeF_4	207	122	10.00	3.2×10^4
TiF_4	124	116	6.32	6.3×10^4
CeF_3	197	114	4.65	4.2×10^4

* Debye temperatures from Refs.13.

a Specific heat at $T = 10\ mK$, in keV $\mathrm{gm}^{-1}\ ^\circ K^{-1}$.

Table 7

Figure of Merit for Crystal Bolometers*

Element	$FM_{el}/10^7$		
	$m = 5\ GeV$	$m = 10\ GeV$	$m = 20\ GeV$
B	323	830	1330
BN	47	122	195
LiF	6.1	19.1	40.8
LiH	4.0	5.3	5.6
Li_20	1.7	3.1	3.7
$LiC\ell$	1.6	6.8	22.3
$LiHF_2$	1.0	3.2	6.9
$A\ell F_3$	2.9	10.3	24.2
VF_3	2.4	10.7	37.5
MgF_2	2.3	8.2	19.3
CaF_2	1.8	6.4	14.9
NaF	1.1	3.8	8.8
NbF_5	0.9	3.3	7.8
ZnF_2	0.9	3.3	7.6
NiF_2	0.7	2.4	5.8
FeF_2	0.7	2.3	5.5
BeF_2	0.6	2.0	4.9

* See Eq. (11). FM_{el} has arbitrary dimensions $(GeV^2 - K^3)$.

Table 8

The Properties and Relative Abundances of some Long-Living Radioisotopes.

Isotope	Type	$t_{1/2}(y)$	Radiation	$E_{\max}(MeV)$	Earth	Element
Th^{232}	A	1.39×10^{10}	α γ	4.0 0.06	10^{-4}	
U^{238}	A	4.5×10^{9}	α γ	4.2 0.048	3×10^{-6}	99.27%
K^{40}	A	1.3×10^{9}	β^- γ	1.32 1.46	3×10^{-4}	0.0118%
U^{235}	A	7.1×10^{8}	α γ	4.82 0.04	2.1×10^{-8}	0.72%
U^{234}	A	1.5×10^{5}	α γ	4.8 0.12	1.7×10^{-9}	0.0057
Th^{230}	A	8×10^{4}	α γ	4.7 0.25	10^{-10}	
Ra^{226}	A	1.62×10^{3}	α γ	4.8 0.64	10^{-12}	
Pa^{231}	A	3.43×10^{4}	α γ	5.0 0.36	10^{-12}	
Sm^{146}	A	5.0×10^{7}	α	2.55	10^{-20}	6.5×10^{-14}
Be^{10}	B	2.7×10^{6}	β^-	0.56	10^{-10}	1.7×10^{-5}
C^{14}	B	5.77×10^{3}	β^-	0.156	10^{-11}	3.1×10^{-8}
Al^{26}	B	7.4×10^{5}	β^+ EC	1.16 2.95	10^{-14}	1.2×10^{-11}
Cl^{36}	B		β^- EC	0.71 1.14	10^{-17}	3.2×10^{-14}
Zr^{93}	C	9.5×10^{5}	β^- γ	0.063 0.029	10^{-14}	4.5×10^{-11}
Cs^{135}	C	2.0×10^{6}	β^- γ	0.21 1.37	10^{-16}	1.42×10^{-11}
I^{129}	C	1.72×10^{7}	β^- γ	0.15 0.040	10^{-16}	3.3×10^{-10}
Tc^{99}	C	2.1×10^{5}	IT	0.096	10^{-17}	
Pd^{107}	C	7.0×10^{6}	β^-	0.035	10^{-17}	10^{-9}
Ca^{41}	D	1.1×10^{5}	EC	0.41	10^{-17}	2.7×10^{-15}
Ni^{59}	D	8.0×10^{4}	EC	1.07	10^{-19}	1.25×10^{-15}
Pb^{205}	D	3.0×10^{7}	EC	0.05	10^{-20}	6.2×10^{-16}
Nb^{96}	D	2.0×10^{4}	β^-	0.5	10^{-21}	4.1×10^{-17}

A Survivors from element formation prior to the formation of the solar system.

B Generated mainly by Cosmic Rays.

C Generated by spontaneous fission of U-238.

D Created by neutron capture.